A Journal of the Gesellschaft Deutscher Chemiker

Angewandte International Edition GDCh Chemie

www.angewandte.org

Accepted Article

Title: High-Performance Ultraviolet Organic Light-Emitting Diode Enabled by High-Lying Reverse Intersystem Crossing

Authors: Han Zhang, Ganggang Li, Xiaomin Guo, Kai Zhang, Bing Zhang, Xuecheng Guo, Yuxuan Li, Jianzhong Fan, Zhiming Wang, Dongge Ma, and Ben zhong Tang

To be cited as: *Angew. Chem. Int. Ed.* 10.1002/anie.202108540

Link to VoR: https://doi.org/10.1002/anie.202108540

WILEY-VCH

High-Performance Ultraviolet Organic Light-Emitting Diode Enabled by High-Lying Reverse Intersystem Crossing

Han Zhang,[a],+ Ganggang Li,[a],+ Xiaomin Guo,[a],+ Kai Zhang,[b] Bing Zhang,[a] Xuecheng Guo,[a] Yuxuan Li,[a] Jianzhong Fan,[b] Zhiming Wang,*[a] Dongge Ma,[a] and Ben Zhong Tang*[a, c]

[a] H. Zhang, G. Li, X. Guo, B. Zhang, X. Guo, Y. Li, Prof. Z. Wang, Prof. D. Ma, Prof. B. Z. Tang
State Key Laboratory of Luminescent Materials and Devices, Guangdong Provincial Key Laboratory of Luminescence from Molecular Aggregates, Center for Aggregation-Induced Emission, AIE Institute
Guangzhou International Campus, South China University of Technology
Guangzhou 510640, China
E-mail: wangzhiming@scut.edu.cn

[b] K. Zhang, J. Fan
Shandong Province Key Laboratory of Medical Physics and Image Processing Technology, School of Physics and Electronics
Shandong Normal University
Jinan 250014, China
E-mail: tangbenz@ust.hk

[c] Prof. B. Z. Tang
Shenzhen Institute of Aggregate Science and Technology, School of Science and Engineering
The Chinese University of Hong Kong, Shenzhen
Shenzhen 518172, China
E-mail: tangbenz@cuhk.edu.cn

[+] These authors contributed equally to this work.

Supporting information for this article is given via a link at the end of the document.

Abstract: Ultraviolet (UV) organic emitters that can open up applications for future organic light-emitting diodes (OLEDs) are of great value but rarely developed. Here, we report a high-quality UV emitter with hybridized local and charge-transfer (HLCT) excited state and its application in UV OLEDs. The UV emitter, 2BuCz-CNCz, shows the features of low-lying locally-excited (LE) emissive state and high-lying reverse intersystem crossing (hRISC) process, which helps to balance the color purity and exciton utilization of UV OLED. Consequently, the OLED based on 2BuCz-CNCz exhibits not only a desired narrowband UV electroluminescent (EL) at 396 nm with satisfactory color purity ($CIE_{x, y}$ = 0.161, 0.031), but also a record-high maximum external quantum efficiency (EQE) of 10.79% with small efficiency roll-off. The state-of-the-art device performance can inspire the design of UV emitters, and pave a way for the further development of high performance UV OLEDs.

Over the last three decades, substantial progress has been made in the development of RGB organic emitters, which makes organic light-emitting diodes (OLEDs) one of the most advanced flat-panel display and solid-state lighting technologies.[1] Nowadays, extending the emission wavelengths of organic emitters to open up new application scenarios for future OLEDs is receiving immense research interest.[2] For instance, OLEDs with ultraviolet (UV) emission (below 400 nm) can find uses in excitation lighting sources,[3] high-density information storage,[4] and chemical/biological sensors.[5] Nevertheless, the electroluminescent (EL) performances of UV OLEDs are still unsatisfactory, and most reported external quantum efficiencies (EQEs) are less than 5%.[2b,6] Therefore, developing high-quality UV organic emitters is extremely urgent yet challenging.

Besides the high requirements for limited π-conjugation, suitable rigidity and coplanarity,[7] the intrinsic wide band-gap of UV emitters usually cause a large carrier-injection barrier and thus reduced carrier combination in OLEDs.[3a,8] A common solution to improve the carrier-injection ability is to construct donor–acceptor (D–A)-type organic emitters.[9] Especially, D–A-type emitters featuring the charge-transfer (CT) state can facilitate the harness of nonradiative triplet excitons via reverse intersystem crossing (RISC),[10] such as the thermally activated delayed fluorescence (TADF) emitters,[1d,11] which is another key to achieving high-performance OLEDs. However, the CT effect can also lead to a bathochromic shift and inferior color purity, making the emission deviate from the UV region. Until recently, the first UV OLED example based on TADF emitter was reported,[6b] reaching the current record maximum EQE of 9.3%, which greatly thrived this research field. Likewise, the broadband UV emission from its low-lying CT-emissive state has a large visible-light component (wavelength region above 400 nm), therefore giving rise to a relatively large CIE *y* coordinate of 0.065. In addition, the device also suffered serious efficiency roll-off at high current densities. Therefore, the design of efficient UV emitters needs further exploration.

D–A-type emitters with a hybridized locally-excited (LE) and CT (HLCT) excited state,[1f,12] in which the CT component promotes the RISC process from the higher-lying triplet states (hRISC), while the low-lying LE-emissive state guarantees the short-wavelength emission, is expected to circumvent the conflict between exciton utilization and color purity in UV emitters. Our previous works reported a long-short axis molecular design for the modulation of LE and CT component in excited state.[13] The strategy concept is illustrated in Figure 1a. The chromophores are connected with small torsion angles to form a LE-emissive long-axis skeleton of the molecule; whereas the electron-withdrawing group is selected as the short-axis skeleton to construct a twisted D–A structure with the long-axis skeleton, and thus introduce the desired CT component. Based on this, we successfully designed a HLCT-type UV emitter, namely 2BuCz-CNCz (Figure 1b). In 2BuCz-CNCz, the chromophores 9-phenyl-9*H*-carbazole are connected in a "head-shoulder-head" pattern to gain the long-short axis skeleton, and the cyano group endows the short-axis skeleton with electron-withdrawing ability. Meanwhile, the branched tert-

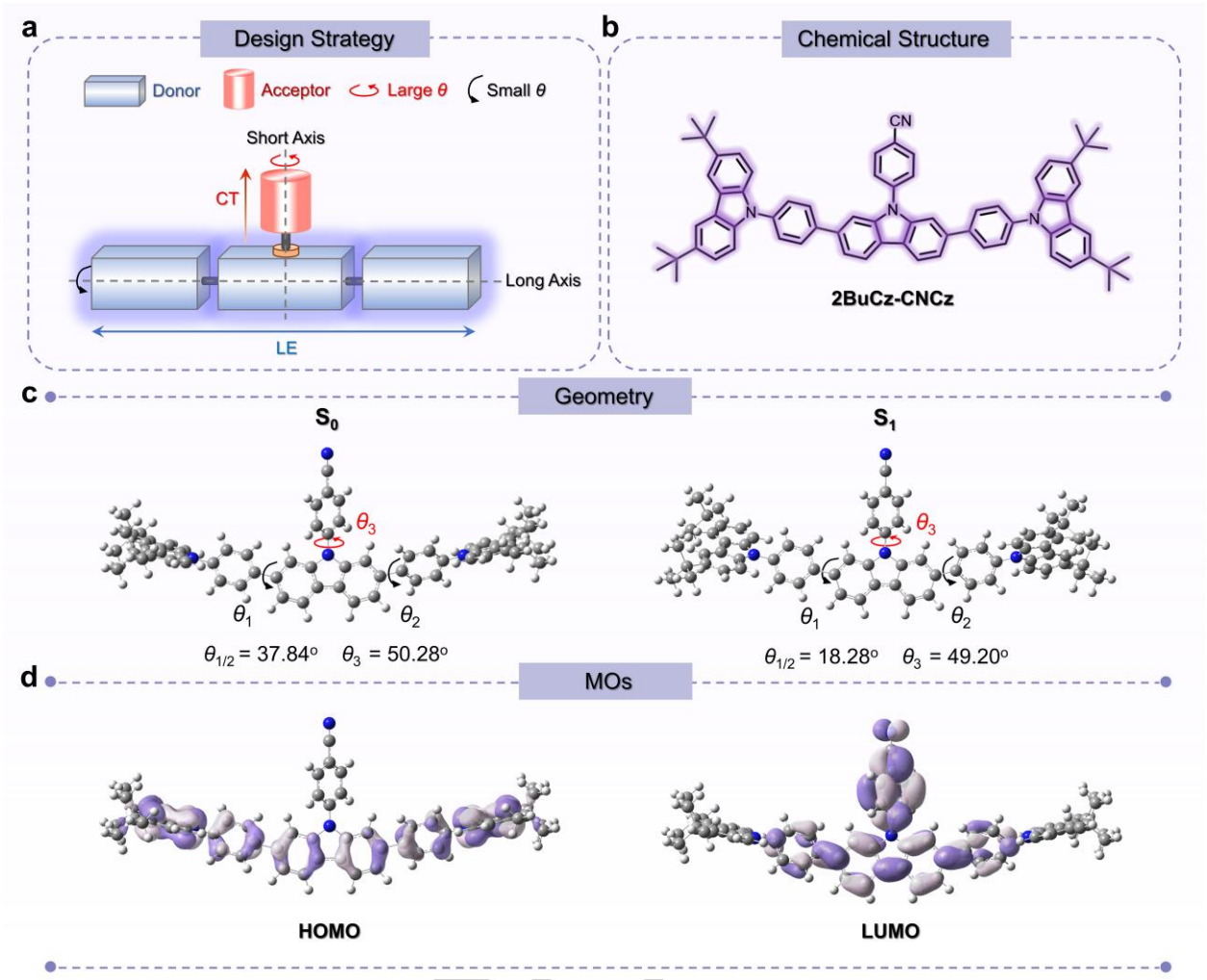

Figure 1. a) Illustration of long-short axis design strategy. b) Chemical structure of 2BuCz-CNCz. c) Optimized S_0 and S_1 geometries, and d) HOMO/LUMO distributions of 2BuCz-CNCz.

butyl groups are inserted to inhibit close molecular packing and alleviate the concentration quenching in aggregates. As a consequence, the doped 2BuCz-CNCz film can emit efficient UV photoluminescence (PL) at 395nm, with a high PL quantum yield (PLQY, η_{PL}) of 70.6 %. Moreover, owing to the contribution of hRISC in the EL process, the UV OLED (396 nm, $CIE_{x,y}$ = 0.161, 0.031) based on 2BuCz-CNCz furnishes an excellent maximum EQE of 10.79% with small efficiency roll-off at high current densities, which represents the state-of-the-art performance of UV OLEDs reported so far.

Density functional theory (DFT) and time-dependent DFT (TD-DFT) simulations were performed to disclose the electronic structure of 2BuCz-CNCz. As designed, the geometries at both S_0 and S_1 states adopt small torsion angles ($\theta_{1/2}$) along the long-axis skeleton, and a larger torsion angle (θ_3) between the central carbazolyl and benzonitrile group (short-axis skeleton) is observed (Figure 1c). The limited changes of $\theta_{1/2}$ and θ_3 indicate that 2BuCz-CNCz possesses good structural rigidity, which is conducive to small Stokes shift and high radiative transition.[14] The highest occupied molecular orbital (HOMO) is thoroughly distributed on the electron-rich multiple carbazolyls as the hole-injection groups (Figure 1d). In comparison, the lowest unoccupied molecular orbital (LUMO) is partially delocalized to the benzonitrile group due to its electron-withdrawing property, reflecting an improvement in electron-injection ability.

The natural transition orbitals (NTO) simulation shows that the “hole” and “particle” of S_1 state are dispersed on the long-axis skeleton with large proportion overlap and partial spatial separation (Figure 2a), which corresponds to a LE-dominant HLCT characteristic. Obviously, the introduction of benzonitrile group has little impact on the luminescence of 2BuCz-CNCz. These results demonstrate the feasibility of our strategy for simultaneously improving the carrier-injection ability and maintaining short-wavelength emission. On the other hand, the lowest T_1 state of 2BuCz-CNCz reveals a pure LE-featured transition with the hole and particle completely overlapped, whereas the high-lying T_2/T_3 states exhibit the HLCT characteristics similar to the S_1 state. In this case, the high-lying CT components could facilitate the triplet-to-singlet conversion from T_2/T_3 to S_1.[1f,2a] As a further proof, the energy level diagrams of 2BuCz-CNCz with the first five singlet and triplet states are calculated (Figure 2b). It can be seen that the energy

Table 1. Photophysical properties of 2BuCz-CNCz.

λ_{abs} [nm]	λ_{PL} [nm]		η_{PL}[c] [%]		$S_1/T_1/\Delta E_{S1T1}$[d] [eV]	$S_1/T_1/\Delta E_{S1T1}$[e] [eV]	$T_2/\Delta E_{S1T2}$[e] [eV]	$T_3/\Delta E_{S1T3}$[e] [eV]
	Soln[a]	Film[b]	Soln[a]	Film[b]				
352	394	410/395	87.6	35.7/70.6	3.34/2.62/0.72	3.26/2.50/0.76	3.11/0.15	3.40/−0.14

[a] Measured in toluene solution (10^{-5} M) at room temperature. [b] Measured in vacuum-deposited neat film/CzSi-hosted film (10 wt% 2BuCz-CNCz). [c] Absolute photoluminescence quantum efficiency evaluated using a calibrated integrating sphere. [d] Estimated from the onsets of the fluorescence and phosphorescence spectra in toluene at 77K. [e] Obtained from the result of theoretical calculations (TD-M062X/6-31G (d, p) calculation).

difference between S_1 and T_1 states (ΔE_{S1T1}) is as large as 0.77 eV, which makes it difficult to induce a sufficient RISC from T_1 to S_1. Nevertheless, a large T_2–T_1 gap (0.61 eV) and small T_2/T_3–S_1 splits (ΔE_{S1T2}: 0.15 eV, ΔE_{S1T3}: –0.14 eV) can be found, providing a new platform for the RISC process from high-lying T_2/T_3 to S_1, namely, hot exciton channel.[15] According to Fermi's golden rule, the spin-orbit coupling (SOC) is another driving force for the occurrence of RISC.[10b,16] Significantly, the values of SOC constants between high-lying T_2/T_3 and S_1 ($\langle S_1\hat{H}_{SO}T_2\rangle$, $\langle S_1\hat{H}_{SO}T_3\rangle$) are also larger than that of $\langle S_1\hat{H}_{SO}T_1\rangle$. Given that the small T_3–T_2 gap supports a dynamic equilibrium of internal conversion (IC) and reverse IC by the vibronic coupling,[17] it is rational that the triplet excitons can be converted into singlet excitons through the hot exciton channels ($T_2/T_3 \rightarrow S_1$).

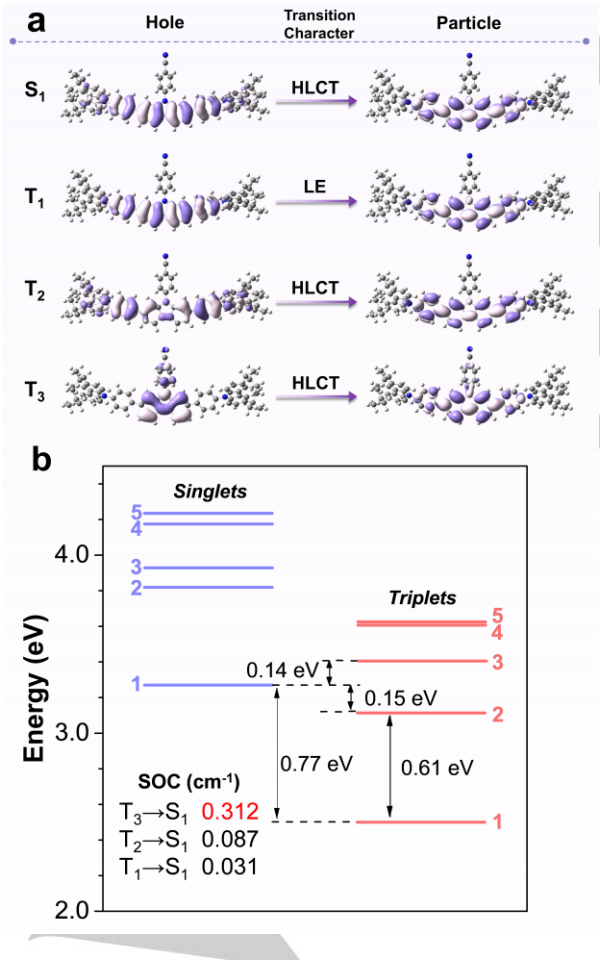

Figure 2. a) NTOs describing the transition characters of the S_1, T_1, T_2 and T_3 states in 2BuCz-CNCz. b) Energy levels of the first five singlet/triplet states and the SOC values between singlets and triplets of 2BuCz-CNCz.

2BuCz-CNCz is facilely prepared in a high yield through the two-steps reactions as described in Scheme S1 in the Supporting Information, and fully characterized by $^1H/^{13}C$ NMR and high-resolution mass spectrometry. It shows good thermal and morphological stabilities, as evidenced by the high decomposition temperature (T_d, 5% weight loss) of 502 °C and high glass-transition temperature (T_g) of 89 °C (Figure S1), which enables the further application in vacuum evaporated OLEDs. The electrochemical properties of 2BuCz-CNCz are investigated by cyclic voltammetry (CV) measurement (Figure S2), and the ionization potentials (IP_{CV}) and electron affinities (EA_{CV}) values are estimated to be 5.36 and 2.30 eV, respectively.

Figure 3a shows the UV-visible absorption and PL spectrum of 2BuCz-CNCz in dilute toluene solution (10^{-5} M). The absorption band at 298 nm can be ascribed to the π–π^* transition of carbazolyl fragment, while the strong and broad absorption band at 352 nm should be caused by the extended π-conjugation of the long-axis skeleton (Figure S3). Upon photoexcitation, 2BuCz-CNCz exhibits a desirable UV emission with PL maxima (λ_{PL}) at 394 nm (Table 1). The small Stokes shift of 42 nm and high PLQY of 87.6 % reflect the suitable molecular rigidity and coplanarity. The solvatochromic effect is used to analyse the excited-state property (Figure 3b and S4). As the solvent polarity increases from *n*-hexane to acetonitrile, the PL spectrum of 2BuCz-CNCz gradually broadens and redshifts from 388 to 422 nm, accompanied by the disappearance of vibronic structures, which implies a substantial change of excited state. Additionally, the Stokes shift (ν_a–ν_f) of 2BuCz-CNCz shows two-section linear relations with the solvent orientational polarizability (f) (Figure 3c). According to the Lippert–Mataga equation,[18] the dipole moment (μ_e) value of the S_1 state is estimated to be 6.1 D in low-polarity solvents ($f \leq 0.167$) and 19.5 D in high-polarity solvents ($f \geq 0.21$), manifesting the LE-featured and CT-featured radiation transition, respectively. It is noteworthy that high PLQYs could be maintained with the increase of solvent polarity (Table S1). Meanwhile, 2BuCz-CNCz exhibits a single-exponential fluorescence decay in each solvent (Figure S5). These two factors indicate that the LE and CT components in 2BuCz-CNCz are well hybridized (HLCT state) rather than simply mixed.

Estimated by the onsets of fluorescence and phosphorescence spectra in frozen toluene (Figure S6), the S_1 and T_1 energy levels of 2BuCz-CNCz are found to be 3.34 and 2.62 eV, respectively, corresponding to ΔE_{S1T1} value as large as 0.72 eV, which is in accord with the theoretical simulation results. After fabricated into neat film, the λ_{PL} of 2BuCz-CNCz shows a redshift to 410 nm with a decreased PLQY of 35.7%, due to the solid-state polarization and aggregation effect[19] (Figure S7). Nevertheless, an efficient UV emission with λ_{PL} at 395 nm and PLQY of 70.6% reappears by dispersing 2BuCz-CNCz into a

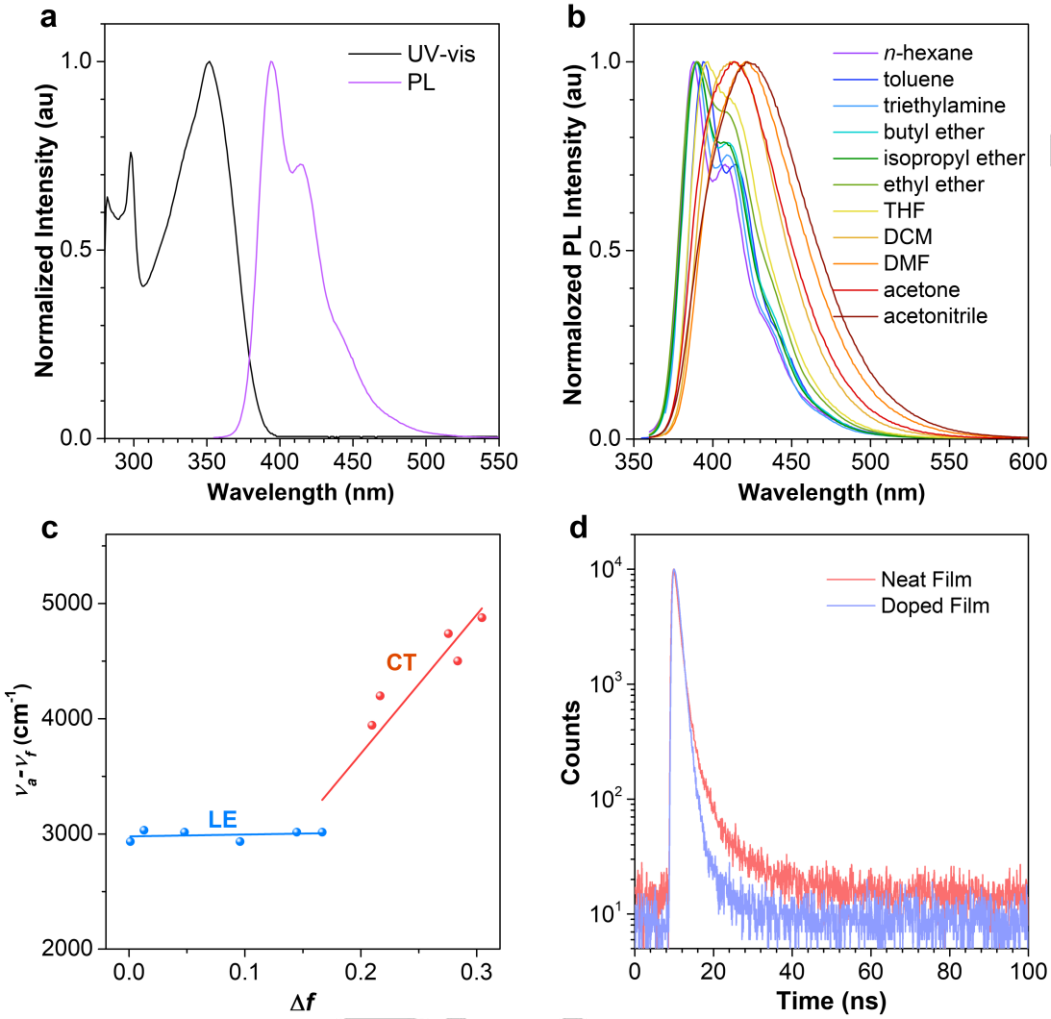

Figure 3. a) UV-visible absorption and PL spectra of 2BuCz-CNCz in toluene (10^{-5} M). b) Solvatochromic PL spectra and c) solvatochromic Lippert–Mataga model of 2BuCz-CNCz. d) Transient PL decay curves of 2BuCz-CNCz in neat film and doped film, respectively, recorded under a N_2 atmosphere at room temperature.

wide band-gap host material CzSi. As depicted in Figure 3d, 2BuCz-CNCz in both neat film and doped film show short fluorescence lifetimes without obvious delay, and the nanosecond-scaled lifetimes are fitted to be 1.9 and 1.3 ns, respectively. Furthermore, temperature-dependent transient PL decay curves reveal the absence of long lifetimes (Figure S8), which can eliminate the possibility of TADF mechanism.

To assess the potential application of 2BuCz-CNCz emitter in UV OLED, a doped device with an optimized configuration of ITO/1,4,5,8,9,11-hexaazatriphenylenehexacarbonitrile (HATCN, 10 nm, hole-injecting layer)/ di-(4-(*N*,*N*-ditolyl-amino)-phenyl)cyclohexane (TAPC, 60 nm, hole-transporting layer)/ tris(4-carbazoyl-9-ylphenyl)amine (TCTA, 5 nm, exciton blocking layer)/CzSi: 2BuCz-CNCz (10%, 20 nm, emitting layer)/ 1,3,5-tris-(N-phenylbenzimidazol-2-yl)benzene (TPBi, 40 nm, electron transporting layer)/LiF (1 nm, electron-injecting layer)/Al (120 nm) is fabricated (**Figure 4**a and Table S2). As expected, the device exhibits a UV EL resembling the PL behavior of the doped film, with a peak wavelength of 396 nm (Figure 4b). Despite the existence of visible-light components in the EL spectrum, the device shows satisfactory color purity due to the narrowband emission (FWHM=33nm), and the CIE coordinates of the device are (0.161, 0.031). Significantly, the device gives a maximum EQE up to 10.79%, which achieves the record-high efficiency of UV OLEDs (Figure 4c). Assuming a light out-coupling efficiency of ITO glass of 20−30%, the corresponding exciton utilization efficiency is calculated to be 51%–76%, which remarkably exceeds the 25% spin statistical threshold of traditional fluorescent OLEDs and reveals the existence of triplet-to-singlet conversion in the EL process. More fascinatingly, the efficiency roll-off of this device is smaller than those of most reported UV OLEDs,[2b] and the EQE maintains a high value of 8.47% at a current density of 10 mA cm^{-2} and 6.8% at 100 mA cm^{-2}, respectively. In addition, the nondoped OLED using neat 2BuCz-CNCz film as the emitting layer is also fabricated (Figure S9), which radiates strong violet-blue EL at 408 nm with CIE coordinates of (0.157, 0.050). Although the PLQY of neat film is decreased as the result of the concentration quenching, the device can furnish a favorable EQE of 5.24%, corresponding to a high exciton utilization efficiency of 53%–79%. Likewise, the

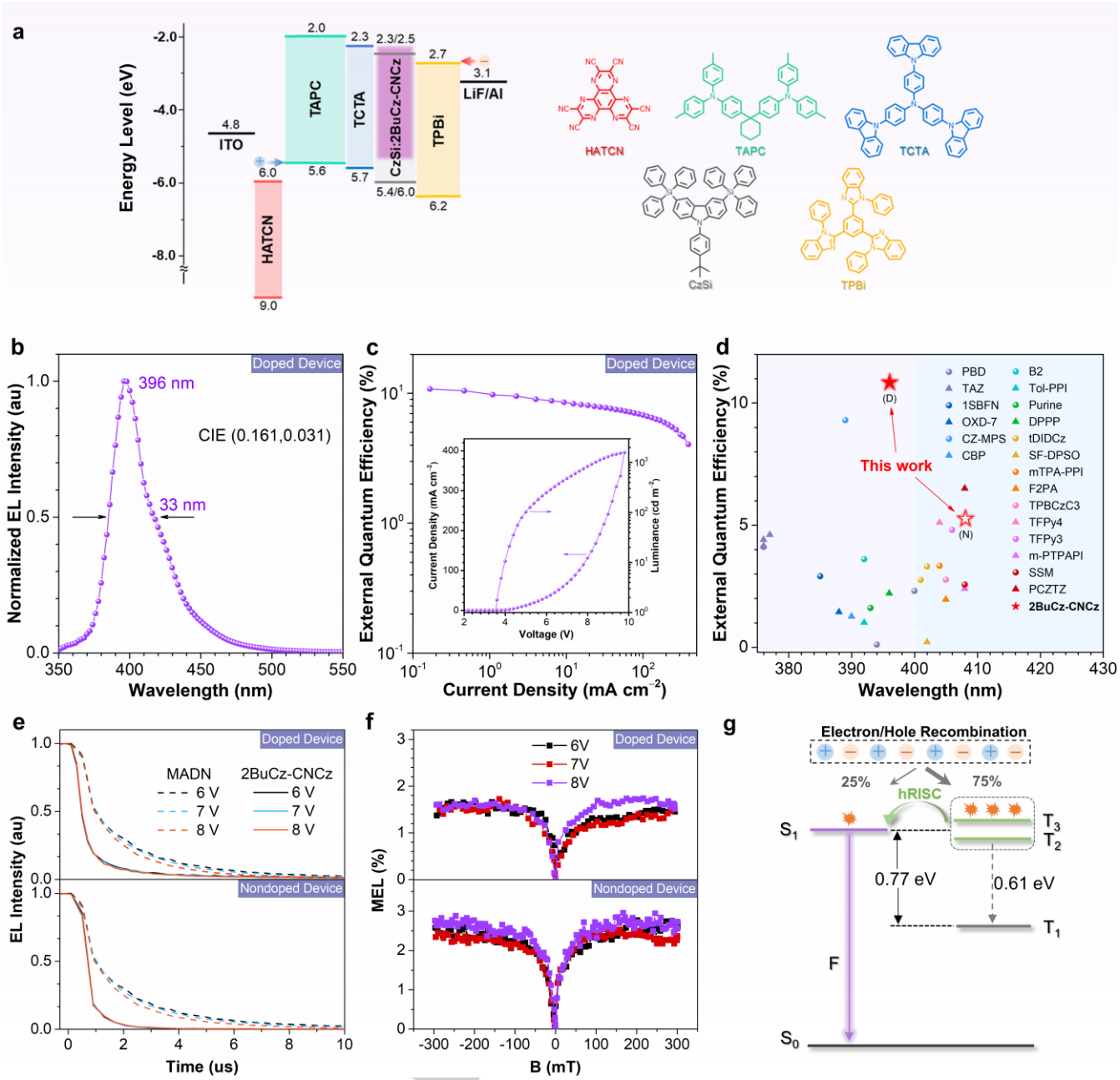

Figure 4. a) Device structure and ionization potentials (IP_{CV}) and electron affinities (EA_{CV}) for each material. b) EL spectrum and c) external quantum efficiency–current density curve of the 2BuCz-CNCz-based UV OLED. Inset shows the current density–voltage–luminance (*J*–*V*–*L*) characteristics. d) External quantum efficiency summary of the representative UV OLEDs (EL Peak ≤ 400 nm) and NUV OLEDs (EL Peak ≤ 410 nm). e) Transient EL decay curves of the MADN (dash line) and 2BuCz-CNCz (solid line) based OLEDs at different voltages. f) MEL curves of the 2BuCz-CNCz-based OLEDs at different voltages.

nondoped device displays a very flat efficiency roll-off (Table S3).To our best knowledge, this is also among the state-of-the-art results of near UV (NUV) OLEDs with a peak wavelength less than 410 nm. The device performances of the representative UV and NUV OLEDs are summarized in Figure 4d and Table S4 in the Supporting Information.

On account of the good linear relationship between the current density and luminance (Figure S10), the breakthrough of the exciton utilization efficiency in both doped and nondoped devices could be not attributed to the triplet−triplet annihilation (TTA) process. The transient EL spectra of the 2BuCz-CNCz-based devices together with a classic TTA-type device based on 2-methyl-9,10-bis(naphthalen-2-yl)anthracene (MADN) are also measured and compared. As shown in Figure 4e, after removing the electrical excitation pulse, the EL intensity of the 2BuCz-CNCz-based both doped and nondoped devices decays much faster than that of the MADN-based one, accompanied by less delayed components. Meanwhile, because of the enhanced triplet excitons quenching process at higher driving voltages, the MADN-based devices exhibit a gradual decrease in the ratio of

delayed component as the driving voltage increases from 6V to 8V; however, the delayed component of the 2BuCz-CNCz-based devices shows almost no voltage dependence, indicating that the delayed response is mainly caused by the collision recombination of trapped charges.[20] These results further exclude the contribution of TTA mechanism in the 2BuCz-CNCz-based devices. On the other hand, the magnetic field effect (MFE) can be used as an effective method to discern the EL mechanism behind OLEDs with efficient triplet exciton utilization.[21] It is noted that the magneto-EL (MEL) traces at varied applied bias present a sharp rise at the low magnetic field (<50 mT) and continuous saturation at the higher magnetic field (Figure 4f), which also demonstrates that the triplet excitons harvesting originates from the RISC rather than TTA process.[15b,22] Since the ΔE_{S1T1} is too large to facilitate the thermally activated RISC process from T_1 to S_1, the triplet states at higher energy level should play a key role in the triplet-to-singlet conversion. Figure 4g illustrates the exciton relaxation path of 2BuCz-CNCz emitter under electrical excitation. After the injected electrons and holes recombine, the singlet and triplet excitons are first formed in a ratio of 1:3 at high energy levels, and then rapidly relax to the low-lying excited states. However, the large energy gap between the higher-lying T_2/T_3 and lowest T_1 can slow down the IC ($T_2/T_3 \rightarrow T_1$) rate according to the energy-gap law,[23] whereas the small energy splitting and enhanced SOC between the T_2/T_3 and S_1 will promote the hRISC process ($T_2/T_3 \rightarrow S_1$). As a consequence, the nonradiative triplet excitons can be converted to S_1 excitons through the fast hot exciton channels before populating into the T_1 state, leading to a high exciton utilization efficiency in the EL devices. Moreover, the triplet involved annihilation processes will be effectively suppressed due to the reduction of the long-lived T_1 excitons concentration. Therefore, a small efficiency roll-off is observed in the 2BuCz-CNCz-based devices.

To summarize, we report a novel UV emitter 2BuCz-CNCz realized by the proposed long-short axis molecular design. This type of D-A structure is proved to enable combined short-wavelength emission and improved carrier-injection ability. The doped 2BuCz-CNCz film possesses a high-quality UV emission, with λ_{PL} at 395 nm and PLQY of 70.6%. Theoretical and experimental investigations also reveal the HLCT characteristic of 2BuCz-CNCz, which can facilitate the triplet-to-singlet conversion via hRISC process ($T_2/T_3 \rightarrow S_1$). As a consequence, the UV OLED based on 2BuCz-CNCz provides a record maximum EQE of 10.79% and a small efficiency roll-off, accompanied by the satisfactory color purity with the EL peak wavelength and CIE coordinates of 396 nm and (0.161, 0.031), respectively. The state-of-the-art performance gained in this work demonstrates the great potential of HLCT emitters with hRISC process, which opens a new avenue for further developing high-performance UV OLEDs.

Acknowledgements

We are grateful for financial support from the National Natural Science Foundation of China (21788102 and 21975077), National Key R&D Program of China (Intergovernmental cooperation project, 2017YFE0132200), Open Research Project of Military Logistics Support Department (BLB19J008), the Fundamental Research Funds for the Central Universities (2019ZD04), Natural Science Foundation of Guangdong Province (2020A1515011542) and Fund of Guangdong Provincial Key Laboratory of Luminescence from Molecular Aggregates (2019B030301003).

Conflict of interest

The authors declare no conflict of interest.

Keywords: organic light-emitting diodes • ultraviolet emission • hybridized local and charge-transfer state • high-lying reverse intersystem crossing • record-high EQE

[1] a) C. W. Tang, S. A. VanSlyke, *Appl. Phys. Lett.* **1987**, *51*, 913; b) Y. Ma, H. Zhang, J. Shen, C. Che, *Synth. Met.* **1998**, *94*, 245; c) M. A. Baldo, D. O'Brien, Y. You, A. Shoustikov, S. Sibley, M. Thompson, S. R. Forrest, *Nature* **1998**, *395*, 151. d) H. Uoyama, K. Goushi, K. Shizu, H. Nomura, C. Adachi, *Nature* **2012**, *492*, 234; e) X. Ai, E. W. Evans, S. Dong, A. J. Gillett, H. Guo, Y. Chen, T. J. H. Hele, R. H. Friend, F. Li, *Nature* **2018**, *563*, 536; f) Y. Xu, P. Xu, D. Hu, Y. Ma, *Chem. Soc. Rev.* **2021**, *50*, 1030.

[2] a) A. Zampetti, A. Minotto, F. Cacialli, *Adv. Funct. Mater.* **2019**, *29*,1807623; b) M. Chen, Y. Liao, Y. Lin, T. Xu, W. Lan, B. Wei, Y. Yuan, D. Li, X. Zhang, *J. Mater. Chem. C* **2020**, 8, 14665; c) S. Chen, H. Xu, *Chem. Soc. Rev.* **2021**, *50*, 8639.

[3] a) T.-C. Chao, Y.-T. Lin, C.-Y. Yang, T. S. Hung, H.-C. Chou, C.-C. Wu, K.-T. Wong, *Adv. Mater.* **2005**, *17*, 992; b) J. Lin, X. Guo, Y. Lv, X. Liu, Y. Wang, *ACS Appl. Mater. Interfaces* **2020**, *12*, 10717.

[4] H. van Santen, J. H. M. Neijzen, *Jpn. J. Appl. Phys.* **2003**, *42*, 1110.

[5] J. Shinar, R. Shinar, *J. Phys. D: Appl. Phys.* **2008**, *41*, 133001.

[6] a) X. Zhang, F. You, S. Liu, B. Mo, Z. Zhang, J. Xiong, P. Cai, X. Xue, J. Zhang, B. Wei, *Appl. Phys. Lett.* **2017**, *110*, 043301; b) Y. Luo, S. Li, Y. Zhao, C. Li, Z. Pang, Y. Huang, M. Yang, L. Zhou, X. Zheng, X. Pu, Z. Lu, *Adv. Mater.* **2020**, *32*, 2001248.

[7] a) K.-T. Wong, Y.-L. Liao, Y.-T. Lin, H.-C. Su, C.-C. Wu, *Org. Lett.* **2005**, *7*, 5131; b) V. Joseph, K. R. J. Thomas, M. Singh, S. Sahoo, J.-H Jou, *Eur. J. Org. Chem.* **2017**, *45*, 6660; c) H. L. Lee, W. J. Chung, J. Y. Lee, *Small* **2020**, *16*, 1907569.

[8] a) H. Liu, Q. Bai, L. Yao, H. Zhang, H. Xu, S. Zhang, W. Li, Y. Gao, J. Li, P. Lu, H. Wang, B. Yang, Y. Ma, *Chem. Sci.* **2015**, *6*, 3797; b) H. Yang, Q. Liang, C. Han, J. Zhang, H. Xu, *Adv. Mater.* **2017**, *29*, 1700553; c) S.-N. Zou, X. Chen, S.-Y. Yang, S. Kumar, Y.-K, Qu, Y.-J. Yu, M.-K. Fung, Z.-Q. Jiang, L.-S. Liao, *Adv. Opt. Mater.* **2020**, *8*, 2001074.

[9] a) Y. Yuan, J.-X. Chen, F. Lu, Q.-X. Tong, Q.-D. Yang, H.-W. Mo, T.-W. Ng, F.-L. Wong, Z.-Q. Guo, J. Ye, Z. Chen, X.-H. Zhang, C.-S. Lee, *Chem. Mater.* **2013**, *25*, 4957; b) M. Liu, X.-L. Li, D. C. Chen, Z. Xie, X. Cai, G. Xie, K. Liu, J. Tang, S.-J Su, Y. Cao, *Adv. Funct. Mater.* **2015**, *25*, 5190.

[10] a) Z. Shuai, D. Beljonne, R. J. Silbey, J. L. Brédas, *Phys. Rev. Lett.* **2000**, *84*, 131; b) P. K. Samanta, D. Kim, V. Coropceanu, J. -L. Brédas, *J. Am. Chem. Soc.* **2017**, *139*, 4042; c) H. Noda, X. -K. Chen, H. Nakanotani, T. Hosokai, M. Miyajima, N. Notsuka, Y. Kashima, J. -L. Brédas, C. Adachi, *Nat. Mater.* **2019**, *18*, 1084.

[11] a) M. Y. Wong, E. Zysman-Colman, *Adv. Mater.* **2017**, *29*, 1605444; b) Y. Im, M. Kim, Y. J. Cho, J. -A. Seo, K. S. Yook, J. Y. Lee, *Chem. Mater.* **2017**, *29*, 1946; c) Y. Liu, C. Li, Z. Ren, S. Yan, M. R. Bryce, *Nat. Rev. Mater.* **2018**, *3*, 18020.

[12] a) L. Yao, S. Zhang, R. Wang, W. Li, F. Shen, B. Yang, Y. Ma, *Angew. Chem. Int. Ed.* **2014**, *53*, 2119; b) W. Li, Y. Pan, R. Xiao, Q. Peng, S. Zhang, D. Ma, F. Li, F. Shen, Y. Wang, B. Yang, Y. Ma, *Adv. Funct. Mater.* **2014**, *24*, 1609; c) B. Li, G. Tang, L. Zhou, D. Wu, J. Lan, L. Zhou, Z. Lu, J. You, *Adv. Funct. Mater.* **2017**, *27*, 1605245; d) J. Yang, Q. Guo, J. Wang, Z. Ren, J. Chen, Q. Peng, D. Ma, Z. Li, *Adv. Opt. Mater.* **2018**, *6*, 1800342; e) C. Fu, S. Luo, Z. Li, X. Ai, Z. Pang, C. Li, K.

Chen, L. Zhou, F. Li, Y. Huang, Z. Lu, *Chem*. *Commun*. **2019**, *55*, 6317; f) X. Chen, D. Ma, T. Liu, Z. Chen, Z. Yang, J. Zhao, Z. Yang, Y. Zhang, Z. Chi, *CCS Chem.* **2021**, *3*, 1285; g) H. Zhang, J. Xue, C. Li, S. Zhang, B. Yang, Y. Liu, Y. Wang, *Adv. Funct. Mater*. **2021**, 2100704; h) Y. Zheng, Z. Wang, X. Wang, J. Li, X. J. Feng, G. He, Z. Zhao, H. Lu, *ACS Appl. Electron. Mater.* **2021**, 3, 422.

[13] a) Z. Wang, Y. Feng, S. Zhang, Y. Gao, Z. Gao, Y. Chen, X. Zhang, P. Lu, B. Yang, P. Chen, Y. Ma, S. Liu, *Phys. Chem. Chem. Phys*. **2014**, *16*, 20772; b) S. Zhang, L. Yao, Q. Peng, W. Li, Y. Pan, R. Xiao, Y. Gao, C. Gu, Z. Wang, P. Lu, F. Li, S.-J. Su, B. Yang, Y. Ma, *Adv. Funct. Mater.* **2015**, *25*, 1755; c) H. Zhang, J. Zeng, W. Luo, H. Wu, C. Zeng, K. Zhang, W. Feng, Z. Wang, Z. Zhao, B. Z. Tang, *J. Mater. Chem. C* **2019**, *7*, 6359; d) H. Zhang, A. Li, G. Li, B. Li, Z. Wang, S. Xu, W. Xu, B. Z. Tang, *Adv*. *Opt*. *Mater*. **2020**, *8*, 1902195. e) H. Zhang, B. Zhang, Y. Zhang, Z. Xu, H. Wu, P. A. Yin, Z. Wang, Z. Zhao, D. Ma, B. Z. Tang, *Adv. Funct. Mater*. **2020**, *30*, 2002323.

[14] W. Yuan, H. Yang, C. Duan, X. Cao, J. Zhang, H. Xu, N. Sun, Y. Tao, W. Huang, *Chem* **2020**, *6*, 1.

[15] a) Y. Pan, W. Li, S. Zhang, L. Yao, C. Gu, H. Xu, B. Yang, Y. Ma, *Adv*. *Opt*. *Mater.* **2014**, *2*, 510; b) Y. Xu, X. Liang, X. Zhou, P. Yuan, J. Zhou, C. Wang, B. Li, D. Hu, X. Qiao, X. Jiang, L. Liu, S. -J. Su, D. Ma, Y. Ma, *Adv*. *Mater*. **2019**, *31*, 1807388; c) Y. Xu, C. Wang, X. Zhou, J. Zhou, X. Guo, X. Liang, D. Hu, F. Li, D. Ma, Y. Ma, *J. Phys*. *Chem*. *Lett*. **2019**, *10*, 6878.

[16] a) D. Beljonne, Z. Shuai, G. Pourtois, J. L. Brédas, *J. Phys. Chem. A* **2001**, *105*, 3899; b) M. K. Etherington, J. Gibson, H. F. Higginbotham, T. J. Penfold, A. P. Monkman, *Nat. Commun.* **2016**, *7*, 13680.

[17] a) Q. Zhang, J. Li, K. Shizu, S. Huang, S. Hirata, H. Miyazaki, C. Adachi, *J. Am. Chem. Soc.* **2012**, *134*, 14706; b) L. Gan, K. Gao, X. Cai, D. Chen, S. -J. Su, *J. Phys*. *Chem*. *Lett*. **2018**, *9*, 4725.

[18] a) W. Li, D. Liu, F. Shen, D. Ma, Z. Wang, T. Feng, Y. Xu, B. Yang, Y. Ma, *Adv*. *Funct*. *Mater*. **2012**, *22*, 2797; b) R. Ieuji, K. Goushi, C. Adachi, *Nat. Commun.* **2019**, *10*, 5283.

[19] Y. He, Z. Qiao, X. Cai, M. Li, W. Li, W. Xie, W. Qiu, L. Wang, S.-J. Su, *ACS Appl. Mater. Interfaces* **2020**, *12*, 49905.

[20] a) X. Tang, Q. Bai, T. Shan, J. Li, Y. Gao, F. Liu, H. Liu, Q. Peng, B. Yang, F. Li, P. Lu, *Adv. Funct. Mater.* **2018**, *28*, 1705813; b) X. Lv, M. Sun, L. Xu, R. Wang, H. Zhou, Y. Pan, S. Zhang, Q. Sun, S. Xue, W. Yang, *Chem. Sci.* **2020**, *11*, 5058.

[21] a) B. Hu, L. Yan, M. Shao, *Adv. Mater.* **2009**, *21*, 1500; b) P. Chen, Z. Xiong, Q. Peng, J. Bai, S. Zhang, F. Li, *Adv. Opt. Mater.* **2014**, *2*, 142.

[22] X. Guo, P. Yuan, J. Fan, X. Qiao, D. Yang, Y. Dai, Q. Sun, A. Qin, B. Z. Tang, D. Ma, *Adv. Mater.* **2021**, 33, 2006953.

[23] M. A. Baldo, D. F. O'Brien, M. E. Thompson, S. R. Forrest, *Phys. Rev*. B **1999**, *60*, 14422.

10.1002/anie.202108540

Entry for the Table of Contents

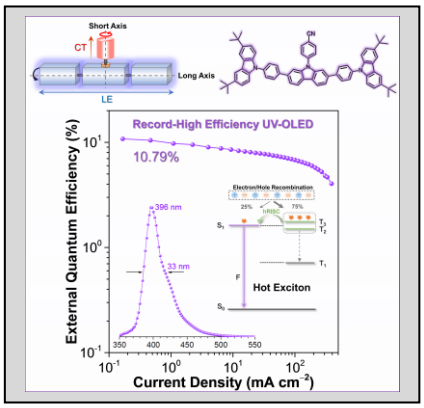

Through the proposed long-short axis molecular design, a novel HLCT-type ultraviolet emitter is reported. Benefiting from the features of the low-lying LE emissive state and high-lying reverse intersystem crossing process, the ultraviolet OLED furnishes a record-high EQE of 10.79%, accompanied by a satisfactory color purity and a small efficiency roll-off.